UNIVERSITÀ DEGLI STUDI DI PADOVA

Dipartimento di Fisica e Astronomia "Galileo Galilei"

Corso di Laurea in Fisica

Tesi di Laurea

Nuclear Structure of ^{33}S using the GALILEO γ-ray spectrometer

Relatore

Prof. Silvia Monica Lenzi

Correlatore

Dr. Dmitry Testov

Laureanda

Anita Candiello

Anno Accademico 2018/2019

Contents

Chapter 1

Introduction

Nuclei are made of two kind of nucleons: (charged) protons and (neutral) neutrons. The nucleons are kept in bound states thanks to the short-range nuclear force. The charged protons however repel each other according to the long-range electromagnetic force. The complex balance of the two forces is explicated in the value of the binding energy of nuclei as a function of the number of protons (Z) and neutrons (N). As nucleons are fermions, the Pauli principle applies, so we can expect that nucleons "build up" the nuclei in some analogy to the atomic electron shell-filling case where some "closed-shell" configurations (Z = 2, 10, 18, 36, 54, 86), corresponding to the noble gases, have higher binding energy. Experiments show indeed that there is more stability for certain ("magic") nuclear numbers Z and N: 2, 8, 20, 28, 50, 82 and 126. These numbers are predicted correctly by the shell model suggested independently by Mayer and Haxel, Jensen and Suess who improved the Wood-Saxon potential by addition of a spin-orbit term. In the nuclear shell model an effective interaction is used. The interaction is valid in a model space that includes the most relevant degrees of freedom of the system under study, above an inert core. It allows computation of the energy levels for nuclei with several valence nucleons outside shell closure, but for nuclei with many valence nucleons the computation of energy levels results unfeasible.

Nuclei in the A $\approx$ 30-40 mass region are a fundamental testing ground for shell-model calculations and effective interactions. The spherical shell model, using the effective interaction (USD), Ref. [1], in the *sd* shell, reproduce with good accuracy the low-spin positive-parity structure of these nuclei. But to describe the negative parity states and the high-spin states, it is necessary to consider a larger valence space involving the excitations of one particle from the *p* to the *fp* shell. For this purpose the PSDPF interaction, Ref. [2], that includes the orbits of three main shells can be used.

In the presented experiment, aimed at the study of high spin states in the ^{33}S nucleus, a fusion-evaporation reaction was used. In these reactions a heavy-ion beam is delivered to a heavy-nucleus stable target forming a compound nucleus at highly excited state and high angular momentum. The compound nucleus then evaporates protons, deuterons, alphas and neutrons in a very fast cooling process (in $\sim 10^{-19}$ s). When the excitation energy of the residual nuclei is below the particles separation energy, these nuclei de-excite by the emission of a cascade of γ rays until they reach their ground states. The study of such γ radiation allowed analysis of energy, spin, parity and lifetimes of the nuclear states. A schematic representation of these reactions is shown in Fig. 1.1.

In this thesis the results of the study of the stable ^{33}S nucleus are presented. High-spin states have been populated via a fusion-evaporation reaction. These states consist not only in excitations within the sd shell, but orbits in the upper fp shell are also involved.
In Chapter 2 the experimental setup which consists of the γ-ray spectrometer GALILEO, the Si-ball EUCLIDES and the Neutron Wall arrays is described. In Chapter 3 the analysis of the experimental data is discussed and the level scheme of ^{33}S constructed with the measured transitions is shown. In

Chapter 4 the experimental levels of ^{33}S are compared with shell model calculations using the PSDPF interaction.

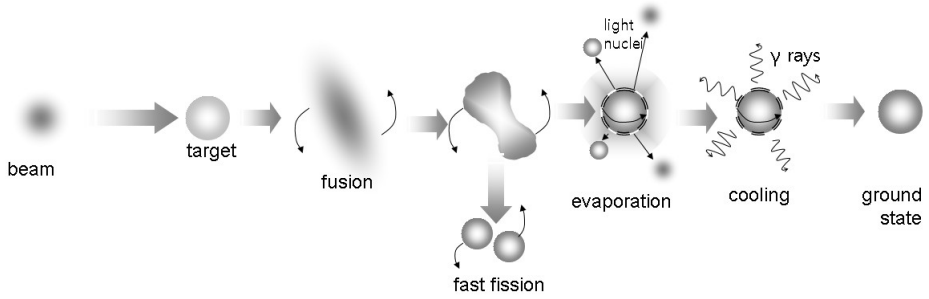

Figure 1.1: Representation of a fusion-evaporation reaction. After the collision, the produced compound nucleus is rapidly rotating and de-excites "evaporating", i.e. emitting light particles. The final residual nucleus cools down to its ground state through γ-emission.

Chapter 2

Experimental details

2.1 Fusion-evaporation reaction

In the discussed experiment excited states in ^{33}S were populated up to 10 MeV via the fusion-evaporation reaction ^{24}Mg(^{12}C, 2p1n)^{33}S using a 45-MeV ^{12}C beam delivered by the Tandem XTU accelerator of the Legnaro National Laboratory. The nucleus of interest was produced after the emission of two protons and one neutron from the ^{36}Ar compound nucleus.

For the γ-ray detection the high-resolution γ-ray spectrometer GALILEO was used. To improve its sensitivity, it was coupled to the Si-ball EUCLIDES and the Neutron Wall. Light charged-particles were detected by EUCLIDES, a 4π silicon-detector array, used for the kinematical reconstruction and for the channel selection. For the last purpose the Neutron Wall, an array of neutron scintillator detectors, was also used.
In order to relate γ rays to the produced nuclei, the three detectors are operated in coincidence. See also [3–6]. Figure 2.1 shows a schematic view of the experimental setup.

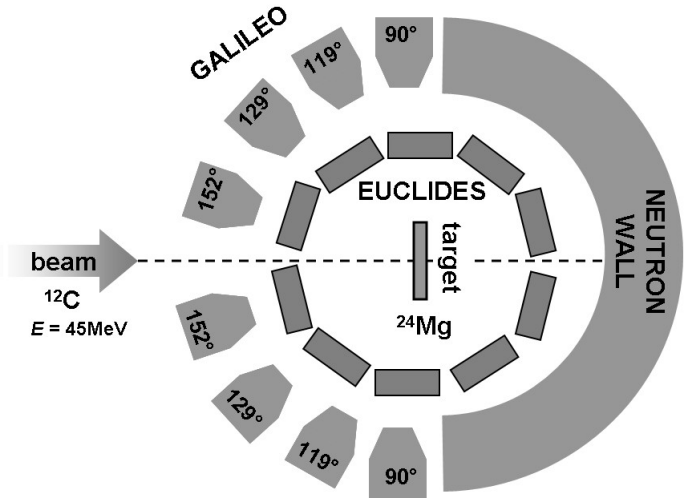

Figure 2.1: Schematic view of GALILEO γ-ray spectrometer coupled to EUCLIDES and to the Neutron Wall arrays. The target is installed at the centre of the reaction chamber.

2.2 GALILEO γ-ray spectrometer

The GALILEO array was composed by 25 high purity / high resolution Ge-detectors (HPGe), arranged in four rings: 5 at 152°, 5 at 129°, 5 at 119° and 10 at 90° with respect to the beam direction. The measured absolute efficiency was ∼2.3% for 1.3 MeV γ ray and the average resolution ∼2.5 keV. The detectors were surrounded by bismuth germanate (BGO) crystals acting as anti-Compton shields, in order to improve the Peak to Total ratio (the number of counts in the photopeak/the total number of counts), that for GALILEO was ∼50%.

The BGO crystals are inorganic scintillators. When a γ event is detect by a BGO in coincidence with an event detected by its HPGe, it means that the photon did not lose all of his energy in the germanium detector but scattered outside the crystal. This imply that the event detected by the HPGe does not contain the complete information on the energy of the photon, but part of it is lost in the BGO. Events like this entail an incorrect estimation of the energy and for this reason must be discarded. In order to avoid the possibility that a photon strikes the scintillator directly, causing possible random coincidences and then the rejection of good events, a thick lead collimator is placed in front of the crystal.

The photo of experimental setup is presented in Figure 2.2, in which the detectors in the 90° ring of the γ-ray spectrometer GALILEO, the Si-ball EUCLIDES and the Neutron Wall are visible.

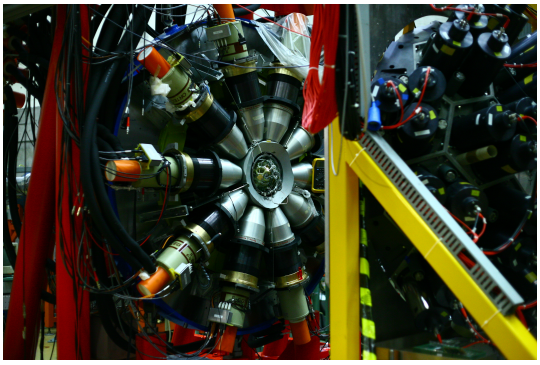

Figure 2.2: Photo of GALILEO γ-ray spectrometer coupled to EUCLIDES and to the Neutron Wall arrays. On the left are visible HPGe detectors inside BGO shield placed at 90° around the reaction chamber. Neutron Wall array, positioned on forward angles with respect to the beam direction, is visible on the right side. The EUCLIDES Si-ball is inserted in the reaction chamber of GALILEO.

A Doppler correction is necessary for the γ rays detected by GALILEO. For this correction, it is assumed that the produced nucleus moves in the same direction of the beam conserving the momentum. Its velocity is then estimated using a mean mass between all possible evaporation channels.

$$E_\gamma = E_\gamma^0 \frac{\sqrt{1-\beta^2}}{1-\beta cos\theta} \approx E_\gamma^0(1+\beta cos\theta) \tag{2.1}$$

where E_γ^0 is the real energy of the emitted γ ray, E_γ is the transition energy in the laboratory, $\beta = \frac{v}{c}$ where v is the velocity of the moving nucleus and c is the speed of light in vacuum, and θ is the angle between the velocity vector and the γ ray direction vector in the laboratory. Supposing that the angle between the velocity vector and the beam axis is negligible we will consider θ to be the angle of the germanium detector with respect to the beam line. The Doppler correction by GALILEO is limited due to the fact that photons are emitted in-flight by recoil nuclei. The γ-ray spectrometer was coupled to the ancillary array EUCLIDES and Neutron Wall to improve this correction by a kinematic reconstruction of the recoil nuclei.

2.3 EUCLIDES array

The Si-ball EUCLIDES array allows detection of light charged particles, essential for the channel selection and for improvement of the correction for the Doppler effect for γ rays using full kinematic reconstruction. The nearly complete 4π coverage of the solid angle ($\sim$80%) and the high granularity of EUCLIDES ensures the high efficiency (60% for protons and 35% for α particles).

EUCLIDES is made up of 40 two-stage ΔE-E telescopes, arranged in a convex polyhedron with 42 faces, 30 hexagons and 12 pentagons. Two pentagonal faces are used for the incoming and outgoing beam ports. The most forward part is composed of 5 hexagonal telescopes electrically segmented in 4 sectors, with equal geometrical area, to sustain a higher counting rate. ΔE and E silicon detectors, that are separated by a 100 μm kapton spacer, have $\sim$130 μm and $\sim$1000 μm thickness and both cover the same $\sim$10.2 cm^2 area. Each telescope is placed at distances $\sim$6.5 cm from the target position. In such configuration EUCLIDES can be inserted in the reaction chamber of GALILEO. The Si-ball EUCLIDES with the ΔE-E telescopes is shown in Figure 2.4.

The light charged particles identification of EUCLIDES relies on the ΔE-E method. The energy loss in the thin ΔE detector is combined with the residual energy detected in the thick E detector, placed behind it. The energy loss of charged ions in matter can be described using the Bethe-Bloch equation [7], in which:

$$\frac{dE}{dx} \propto \frac{mZ^2}{E} \tag{2.2}$$

where $\frac{dE}{dx}$ is the differential energy loss for the particles within the material divided by the corresponding differential path length dx and the energy E, the mass m and the atomic number Z refer to the incident particles. Plotting the energy loss versus the residual energy, the events will be distributed among different loci, each one corresponding to different values of mZ^2. Using telescopes, it is possible both to discriminate between particles and to measure their total energy. To perform good energy measurements, the E detector should be thick enough to stop particles. However, even if a particle is not stopped in the E detector, it can be still identified using the energy released in the telescope.

Figure 2.3 shows a schematic illustration of a two-stage ΔE-E silicon telescope of EUCLIDES and a two dimensional correlation plot of the energy loss ΔE versus the residual energy E that allows to identify the light charged particles. The events corresponding to protons, deuterons and alpha particles can be clearly distinguished.

A further correction for the Doppler effect of γ rays detected by GALILEO can be improved by EUCLIDES. By detecting θ and the energy E of of the light particles α, p, n, the trajectory of the residual nucleus can be reconstructed. According to Eq. 2.1 it can be seen that the loss of resolution of the γ-ray spectrometer, $\frac{E_\gamma - E^0_\gamma}{E_\gamma}$, comes from two components, originating from the dispersion in the recoil velocity β and in the angle θ between the direction of the photons emitted and the direction of the recoil nucleus. Since momentum is conserved, the evaporation of particles induces a spread in the velocity of the residual nuclei and in their direction. The conservation of momentum is:

$$\vec{p}_{residual} = \vec{p}_{compound} - \sum_{i=1}^{N} \vec{p_i} \tag{2.3}$$

where $\vec{p}_{residual}$ is the momentum of the residual nucleus, $\vec{p}_{compound}$ is the momentum of the compound nucleus and $\vec{p_i}$ are the momenta of the N single particles evaporated from the compound nucleus. Detecting the evaporated light particles it is possible to perform the kinematic reconstruction of the velocity of the recoiling nucleus, thus allowing a more precise correction for the Doppler effect.

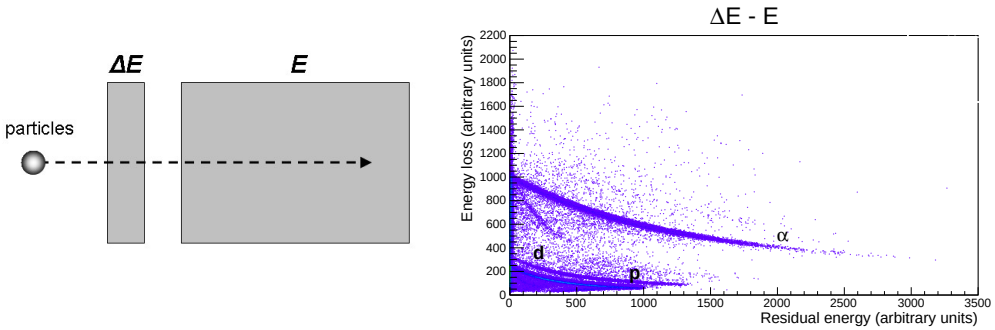

Figure 2.3: On the left a schematic illustration of ΔE-E EUCLIDES detector is shown. On the right the energy loss ΔE vs residual energy E plot for light charged particles identification is shown.

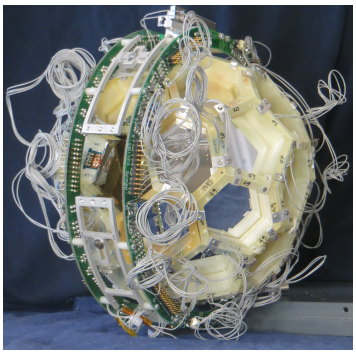

Figure 2.4: EUCLIDES Si-ball array at Legnaro National Laboratory (LNL)

2.4 Neutron Wall detector

The Neutron Wall is an ancillary detector of GALILEO used to detect neutrons and, coupled to EUCLIDES, necessary to select channel in fusion evaporation reactions. Considering a solid angle coverage of 1π, the efficiency of Neutron Wall to detect one neutron is $\sim$ 20-25%.

The Neutron Wall is composed of 46 liquid scintillator detectors coupled to Photo Multiplier Tubes (PMT) set at forward angles with respect to the beam direction.
Neutrons excite electrons of the material molecules that, during the de-excitation process, emit (visible) photons that are subsequently collected and converted into an electrical signal by the photomultipliers.

Scintillator detectors can detect both neutrons and γ rays. In order to discriminate between them, there are two main methods: the Pulse Shape Analysis (PSA) and the Time of Flight (TOF) technique. Using the Zero Cross Over (ZCO) pulse shape technique, neutrons and γ rays can be discriminated according to the different decay time of signals produced in scintillators. Neutrons have lower velocity with respect to electromagnetic radiation and therefore the time of flight (TOF) for γ rays and neutrons (emitted almost simultaneously in the evaporation process) from the reaction point to the detector is different. Neutrons and γ rays can be also identified knowing that neutrons have a higher energy loss $\frac{dE}{dx}$ in detection material with respect to photons.

Chapter 3

Data Analysis and results

Considering the symmetric E_γ-E_γ matrix, in which both x and y axis represent the energies of γ rays detected by all the detectors, only the γ rays in coincidence with two protons and one neutron were incremented. By observing several γ-ray projections on the matrix, the level scheme of ^{33}S was constructed.

3.1 Experimental results

The relative intensities of the γ-ray transitions were measured relative to the intensity of the γ-ray transition at 1968 keV using single γ-ray spectrum. The photopeak efficiency of a detector varies with the photon energy, therefore, to extract the relative intensity, measured areas were corrected by absolute efficiency. For the i-th transition the relative intensity I^i_γ was obtained as:

$$I^i_\gamma = \frac{\frac{A^i_\gamma}{\varepsilon^i_\gamma}}{\frac{A_{1968}}{\varepsilon_{1968}}} = \frac{A^i_\gamma}{A_{1968}} \frac{\varepsilon_{1968}}{\varepsilon^i_\gamma} \tag{3.1}$$

being A^i_γ and ε^i_γ the area of the peak and the efficiency, respectively, corresponding to the i-th transition while A_{1968} and ε_{1968} the area and the efficiency of the 1968-keV γ-ray. The I_γ errors were calculated using the error propagation formula *. All the values were then multiplied by a factor 1000.

When a low-intensity transition was not visible in single γ-ray spectrum, its relative intensity was measured using E_γ-E_γ matrices.

The absolute efficiency was measured using standard calibration sources ^{152}Eu and ^{60}Co. The efficiency of germanium detectors is highly dependent on the energy of the detected γ-ray. The energy region in which they are most efficient is around 100 keV, while their performances worsen at high energy because the probability that a photon escapes the crystal without losing its entire energy is larger. The measured curve of the efficiency, a function of photons energy (E_γ), was described by Eq.3.2:

$$\varepsilon(E_\gamma) = \frac{P_0 + P_1 ln(E_\gamma) + P_2 ln^2(E_\gamma) + P_3 ln^3(E_\gamma)}{E_\gamma} \tag{3.2}$$

where $P_0 = (-597 \pm 44)$, $P_1 = (78 \pm 10)$, $P_2 = (23 \pm 2)$, $P_3 = (2.2 \pm 0.2)$ are the fitting parameters.

* $\sigma^2_{I_\gamma} = (\frac{\varepsilon_{1968}}{\varepsilon^i_\gamma A_{1968}})^2 \sigma^2_{A^i_\gamma} + (\frac{A^i_\gamma}{A_{1968}\varepsilon^i_\gamma})^2 \sigma^2_{\varepsilon_{1968}} + (\frac{A^i_\gamma \varepsilon_{1968}}{\varepsilon^i_\gamma A^2_{1968}})^2 \sigma^2_{A_{1968}} + (\frac{A^i_\gamma \varepsilon_{1968}}{A_{1968}\varepsilon^{i\,2}_\gamma})^2 \sigma^2_{\varepsilon^i_\gamma}$

Errors were calculated using the error propagation formula †.

By measuring the intensity of a γ-ray transition as a function of the detection angle it was possible to assign different multipolarity to transitions and therefore to extract information about the spin and parity of the de-exciting state. Where possible, ADO ratios (γ-ray Angular Distribution from Oriented nuclei) were measured. For this purpose two ad hoc E_γ-E_γ matrices, having on the first axis the detectors at ring 90° and 152° respectively and on the second axis all the other detectors, were produced. Measured γ ray intensities, corrected for efficiency, were used to calculate the ADO ratio (R_{ADO}) defined as:

$$R_{ADO} = \frac{I_{\gamma_1}^{152^\circ}}{I_{\gamma_1}^{90^\circ}} = \frac{A_{\gamma_1}^{152^\circ}}{\varepsilon_{\gamma_1}^{152^\circ}} \frac{\varepsilon_{\gamma_1}^{90^\circ}}{A_{\gamma_1}^{90^\circ}} \tag{3.3}$$

where $I_{\gamma_1}^{152^\circ}$ and $I_{\gamma_1}^{90^\circ}$ are the intensities of γ_1 rays (corrected by efficiency) collected by detectors at 152° and 90° and in coincidence with γ_2 ray which is measured by all detectors. $A_{\gamma_1}^{152^\circ}$, $A_{\gamma_1}^{90^\circ}$ and $\varepsilon_{\gamma_1}^{152^\circ}$, $\varepsilon_{\gamma_1}^{90^\circ}$ are the areas of the peaks and the efficiencies of γ_1 ray measured. For R_{ADO} errors, the error propagation formula was used *.

The gates were set on the transitions with higher intensities: 1968 keV, 2970 keV, 1639 keV, 968 keV, 1932 keV. For straight dipole transitions was obtained $R_{ADO} \sim 0.9$ and $R_{ADO} \sim 1.8$ for straight quadrupole ones.

Measured transition energies, Level energies, R_{ADO} ratios and multipolarities, where possible, are reported in Table 3.1. For E_γ errors, both statistical and systematic (0.5keV) errors were considered. The spin-parity assignments are taken from Ref.[8]. In the Table 3.2 are reported the values of the measured branching ratios (BR). Considering the γ rays de-exciting a nuclear level, their relative intensities were obtained by gating in a γ ray feeding the level of interest. An intensity of 100 is assumed for the most intense transition.

Table 3.1: γ-ray transitions and level energies in ^{33}S observed in the present experiment. Spin-parity assignment for initial and final states is from Ref.[8]. Relative intensities of γ-rays, R_{ADO} and multipolarities measured in the present work are indicated.

E_{level}(keV)	J_i^π	J_f^π	E_γ(keV)	I_γ^{rel}	R_{ADO}	*Multipolarity*
841.4(5)	$1/2^+$	$3/2^+$	841.4(5)	79(7)		
1967.8(5)	$5/2^+$	$1/2^+$	1127.0(6)	14(5)		
		$3/2^+$	1967.8(5)	1000(81)		
2936.2(7)	$7/2^-$	$5/2^+$	968.4(5)	528(46)	0.92(30)	$E1$
		$3/2^+$	2937.4(10)	370(100)		
2969.5(6)	$7/2^+$	$5/2^+$	1002.2(5)	36(4)	1.10(49)	$M1$
		$3/2^+$	2969.5(6)	400(77)		
4049.8(8)	$9/2^+$	$7/2^+$	1078.6(6)	35(4)	0.39(28)	
		$7/2^-$	1113.6(8)	15(6)		
		$5/2^+$	2082.0(6)	194(21)	1.89(61)	$E2$

Continued on next page

† $\sigma^2_{\varepsilon(E_\gamma)} = (\sigma^2_{P_0} + ln^2(E_\gamma)\sigma^2_{P_1} + ln^4(E_\gamma)\sigma^2_{P_2} + ln^6(E_\gamma)\sigma^2_{P_3})\frac{1}{(E_\gamma)^2} + [(P_1 + 2P_2 ln(E_\gamma) + 3P_3 ln^2(E_\gamma)) - (P_0 + P_1 ln(E_\gamma) + P_2 ln^2(E_\gamma) + P_3 ln^3(E_\gamma))]^2 \frac{\sigma^2_{E_\gamma}}{(E_\gamma)^4}$

* $\sigma^2_{R_{ADO}} = (\frac{\varepsilon^{90^\circ}_{\gamma_1}}{\varepsilon^{152^\circ}_{\gamma_1} A^{90^\circ}_{\gamma_1}})^2 \sigma^2_{A^{152^\circ}_{\gamma_1}} + (\frac{A^{152^\circ}_{\gamma_1}}{A^{90^\circ}_{\gamma_1} \varepsilon^{152^\circ}_{\gamma_1}})^2 \sigma^2_{\varepsilon^{90^\circ}_{\gamma_1}} + (\frac{A^{152^\circ}_{\gamma_1} \varepsilon^{90^\circ}_{\gamma_1}}{\varepsilon^{152^\circ}_{\gamma_1} A^{90^\circ 2}_{\gamma_1}})^2 \sigma^2_{A^{90^\circ}_{\gamma_1}} + (\frac{A^{152^\circ}_{\gamma_1} \varepsilon^{90^\circ}_{\gamma_1}}{A^{90^\circ}_{\gamma_1} \varepsilon^{152^\circ 2}_{\gamma_1}})^2 \sigma^2_{\varepsilon^{152^\circ}_{\gamma_1}}$

Table 3.1 – *Continued from previous page*

E_{level}(keV)	J_i^π	J_f^π	E_γ(keV)	I_γ^{rel}	R_{ADO}	$Multipolarity$
4095.9(11)	$7/2^+$	$5/2^+$	2128.1(10)	56(8)	1.24(46)	$M1+M2$
4730.4(8)	$9/2^-$	$7/2^+$	1760.9(6)	198(18)	0.85(30)	$E1$
		$7/2^-$	1794.3(6)		1.97(86)	$M1+E2$
4868.1(9)	$11/2^-$	$7/2^-$	1931.9(5)	665(55)	1.82(58)	$E2$
5477.7(11)	$9/2^-$	$11/2^-$	610.5(10)			
		$9/2^-$	747.3(7)	14(4)		
		$7/2^+$	1382.4(11)	53(7)		
		$7/2^+$	2507.9(3)			
		$7/2^-$	2542.4(8)	37(4)		
5721.8(10)	$9/2^+$	$9/2^+$	1672.0(6)			
6523.8(11)	$11/2^-$	$9/2^-$	1793.4(7)	31(7)		
7001.1(19)	$11/2^+$	$9/2^+$	1279.3(16)			
		$9/2^-$	1520.7(7)	41(5)		
		$11/2^-$	2132.7(14)			
		$9/2^-$	2270.5(10)	13(4)		
		$9/2^+$	2951.1(14)			
7180.9(13)	$13/2^-$	$11/2^-$	2312.8(9)	55(13)	2.15(86)	$M1+E2$
		$9/2^-$	2451.0(9)	28(3)		
7573.8(14)	$13/2^-$	$13/2^-$	392.9(6)	6(1)		
		$9/2^-$	2098.4(11)			
		$11/2^-$	2709.4(14)	22(3)		
		$9/2^-$	2847.1(12)	52(6)		
7818.0(14)	$15/2^-$	$13/2^-$	637.1(6)			
		$15/2^-$	2949.9(17)			
8640.6(20)	$15/2^+$	$13/2^-$	1065.3(7)	70(11)		
		$13/2^-$	1457.5(15)			
		$11/2^+$	1639.5(5)	86(8)		
9815.7(21)	$17/2^+$	$15/2^+$	1175.1(6)	48(5)	0.84(61)	

Table 3.2: Level energies, E_γ and branching ratios (BR) measured in the present work, spin-parity assignments are taken from Ref.[8].

E_i(keV)	J_i	E_γ(keV)	$BR(\%)$	E_f(keV)	J_f
841.4(5)	$1/2^+$	841.4(5)	100	0	$3/2^+$
1967.8(5)	$5/2^+$	1127.0(6)	1.0(2)	841.4(5)	$1/2^+$
		1967.8(5)	100(11)	0	$3/2^+$
2936.2(7)	$7/2^-$	968.4(5)	100(18)	1967.8(5)	$5/2^+$
		2937.4(10)	70(13)	0	$3/2^+$
2969.5(6)	$7/2^+$	1002.2(5)	9(1)	1967.8(5)	$5/2^+$
		2969.5(6)	100(11)	0	$3/2^+$
4049.8(8)	$9/2^+$	1078.6(6)	30(20)	2969.5(6)	$7/2^+$
		2082.0(6)	100(60)	1967.8(5)	$5/2^+$

Continued on next page

Table 3.2 – *Continued from previous page*

E_i(keV)	J_i	E_γ(keV)	BR(%)	E_f(keV)	J_f
4095.9(11)	$7/2^+$	2128.1(1)	100	1967.8(5)	$5/2^+$
4730.4(8)	$9/2^-$	1760.9(6)	100(37)	2969.5(6)	$7/2^+$
		1794.3(6)	15(8)	2936.2(7)	$7/2^-$
4868.1(9)	$11/2^-$	1931.9(5)	100	2936.2(7)	$7/2^-$
5477.7(11)	$9/2^-$	1382.4(11)	45(23)	4095.9(11)	$7/2^+$
		2507.9(3)	100(49)	2969.5(6)	$7/2^+$
		2542.4(8)	72(40)	2936.2(7)	$7/2^-$
5721.8(10)	$9/2^+$	1672.0(6)	100	7180.9(13)	$13/2^-$
6523.8(11)	$11/2^-$	1793.4(7)	100	4730.4(8)	$9/2^-$
7001.1(19)	$11/2^+$	1520.7(7)	44(24)	5477.7(11)	$9/2^-$
		2270.5(10)	60(28)	4730.4(8)	$9/2^-$
		2951.1(14)	100(57)	4049.8(8)	$9/2^+$
7573.8(14)	$13/2^-$	392.9(6)	12(4)	7180.9(13)	$13/2^-$
		2098.4(11)	100(22)	5477.7(11)	$9/2^-$
		2709.4(14)	26(8)	4868.1(9)	$11/2^-$
		2847.1(12)	42(22)	4730.4(8)	$9/2^-$
8640.6(20)	$15/2^+$	1065.3(7)	66(17)	7573.8(14)	$13/2^-$
		1639.5(5)	100(26)	7001.1(19)	$11/2^+$
9815.7(21)	$17/2^+$	1175.1(6)	100	8640.6(20)	$15/2^+$

3.2 The level scheme of ^{33}S

In a fusion-evaporation reaction the residual nuclei are populated in states of high excitation energy and angular momentum. These nuclei subsequently decay to discrete states with lower energy and lower angular momentum until the ground state is reached. Decays occurs through discrete γ-ray transitions, whose energy corresponds to the energy difference between the excited states. The coincident windows for γ rays and particles used in the reported experiment was $\sim$40 ns.

The odd-mass isotope ^{33}S, with 16 protons and 17 neutrons, was populated via 2p1n evaporating channel from the compound nucleus ^{36}Ar. The level scheme of ^{33}S was constructed on the basis of coincident relationships in spectra obtained with appropriate gates on the symmetric E_γ - E_γ matrices. Starting from the E_γ - E_γ matrix projection by gating on the energy of one of the γ-ray transitions of the nucleus the other γ rays in coincidence were observed.

Figure 3.1 illustrates E_γ - E_γ background-subtracted coincidence spectra obtained by gating on the γ rays at 1968 keV (a), 968 keV (b), and 1932 keV (c) which depopulate the low-lying states in ^{33}S, as well as the 1175 keV (e), 1639 keV (f) and 1065 keV (g) transitions de-exciting higher-lying levels. In Figure 3.1 panels (d) and (h) correspond to the sum of the projections of E_γ - E_γ matrix gated on 1968 keV - 968 keV - 1932 keV (d) and 1175 keV - 1639 keV - 1065 keV (h). In these spectra several transitions of other contaminant nuclei appear. This will be discussed in more detail in Section 3.3.

The resulting level scheme of ^{33}S is shown in Figure 3.2. The widths of the arrows correspond to the relative intensities reported in Table 3.1. Where it was not possible to measure the intensity of a transition, it was assigned the value of 1/10 of that of the highest intensity (the 1968-keV γ-ray

transition). All the γ-rays observed previously were confirmed in the present study with the exception of some γ-ray transitions at low intensities, due to statistic.

It was observed that the π^+ high-spin levels $J^\pi=15/2^+$ (at 8641 keV) and $J^\pi=11/2^+$ (at 7001 keV), decay through negative parity states. Thus the 1065 keV transition feeds the $13/2^-$ level while the γ rays at 2271 keV, 2133 keV and 1521 keV γ-rays populate respectively yrast $9/2^-$, $11/2^-$ and no-yrast $9/2^-$ states. The $9/2^-$ yrast level (at 4730 keV) de-excites by the 1761 keV transition feeding $7/2^+$ state (at 2970 keV). Furthermore, the intense 968 keV transition links the negative parity $7/2^-$ at 2936 keV and the positive-parity $5/2^+$ level at 1968 keV. The intensity of γ-ray transitions linking the positive-parity states is lower than the intensity passing through negative-parity levels.

3.3 Selectivity of experimental setup

One of the key-feature of the modern γ-ray spectrometers, such as GALILEO at LNL, is their capability to identify and to study exotic excited states produced at very low cross sections. The use of ancillary detectors, to improve the selectivity of a γ spectrometer, can help to detect rare exotic process at much higher resolving power than simple γ-detection. Since in a fusion-evaporation reaction various species are produced in different evaporation channels, simultaneous detection of evaporated light particles (α, proton, deuteron, etc.) and emitted γ-rays allows to attain the maximum selectivity.

The reaction ^{12}C(45 MeV) + ^{24}Mg populated several nuclei with different cross sections. The most populated nuclei in this experiment were ^{31}P[1α1p] ($\sim$35%), ^{33}S[2p,1n] ($\sim$18%), ^{28}Si[2α] ($\sim$13%), ^{27}Al[2α1n] ($\sim$10%), ^{30}P[1α1p1n] ($\sim$7%), ^{34}Cl[1p1n] ($\sim$6%), ^{31}S[1α1n] ($\sim$4%), ^{34}S[2p] ($\sim$3%). In the present experiment for the channel selection EUCLIDES (see Section 2.3) for the light particles and the Neutron Wall (see Section 2.4) for the detection of neutrons were used.

Figure 3.3 shows four examples of the full projection of γ-γ matrices requiring coincidence with various combinations of protons, α particles and neutron. In the panel (a) it is shown a spectrum recorded requesting two protons an one neutron coincidence. The transitions of 968 keV and 1968 keV of ^{33}S dominate. Such transitions in the γ-ray spectrum recorded with 1α gate (b) are suppressed while 1266 keV of ^{31}P, produced via 1α1p evaporation channel, dominates. A further selectivity of ^{31}P can be achieved by imposing 1α1p gate.

In the spectrum recorded requesting 2p1n coincidence, see Fig. 3.3(a), most of the γ rays were attributed to transitions in ^{33}S. However we noticed that different transitions from contaminant nuclei are also present in the spectrum: 491 keV (^{34}Cl[1p1n]), 709 keV (^{30}P[1α1p1n]), 1266 keV (^{31}P[1α1p] and ^{30}P[1α1p1n]), 2234 keV (^{31}P[1α1p] and ^{30}S[1α2p]), 1002 keV, 1066 keV, 1127 keV, 1177 keV, 1320 keV, 2561 keV, 2680 keV and 3304 keV (^{34}S[2p] see Ref.[10]).

This is due to two main factors. The efficiency of the Si-ball EUCLIDES and the Neutron Wall is less than 100%. When two proton and one neutron coincidence is requested it can happen that a neutron or a proton of an other residual nucleus is not detected and the γ-ray transitions of the nucleus comes in the spectrum in analysis, contaminating it. It can also happen that the contamination correspond to the misidentification of a neutron as a γ ray related to the properties of γ-n discrimination.

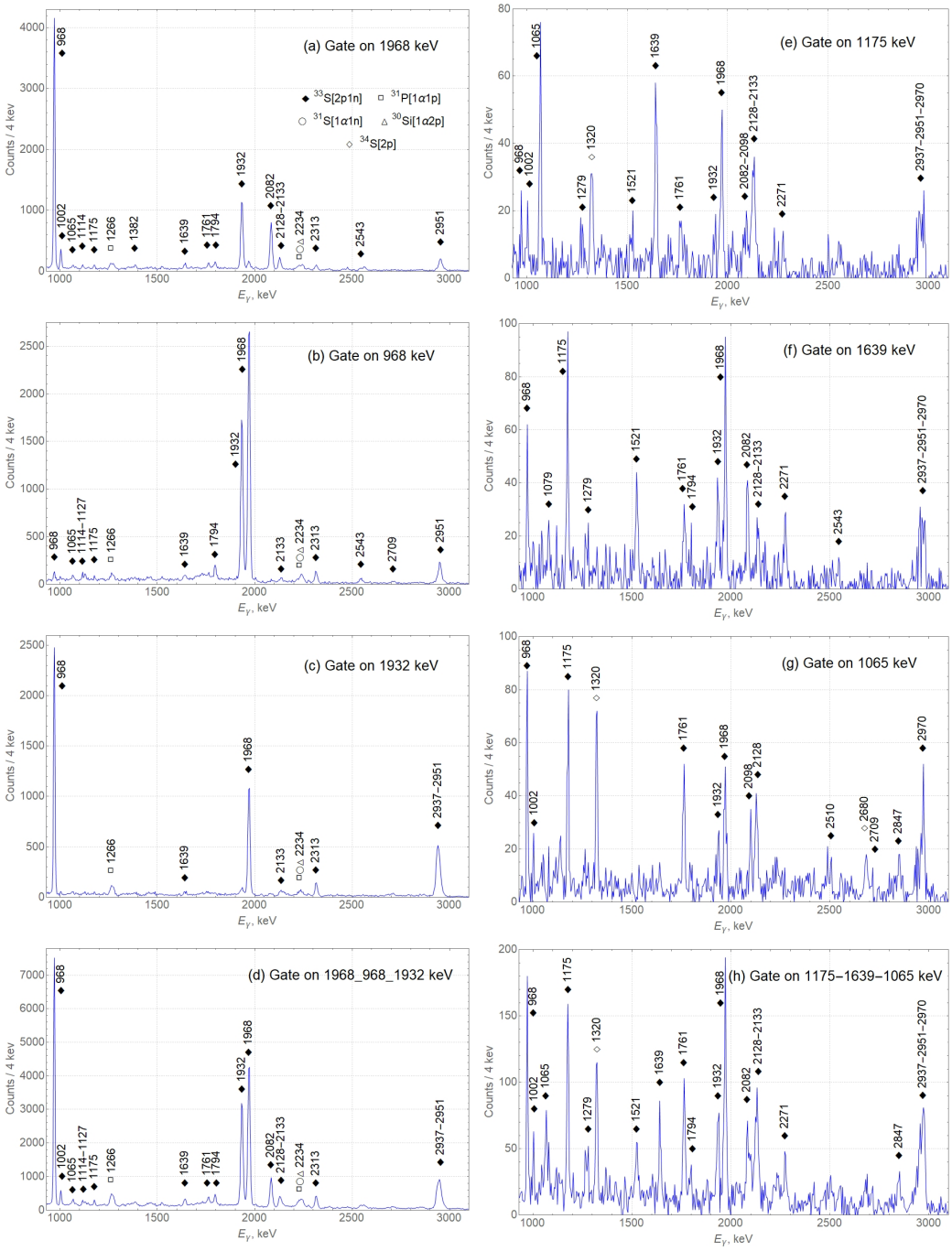

Figure 3.1: Background-subtracted coincident spectra obtained from the $E_\gamma - E_\gamma$ matrix gating on γ-ray transitions at 1968 keV (a), 968 keV (b), and 1932 keV (c), 1175 keV (e), 1639 keV (f) and 1065keV (g) and spectra obtained by the sum of the projections on 1968 keV - 968 keV - 1932 keV (d) and 1175 keV - 1639 keV - 1065 keV (h).

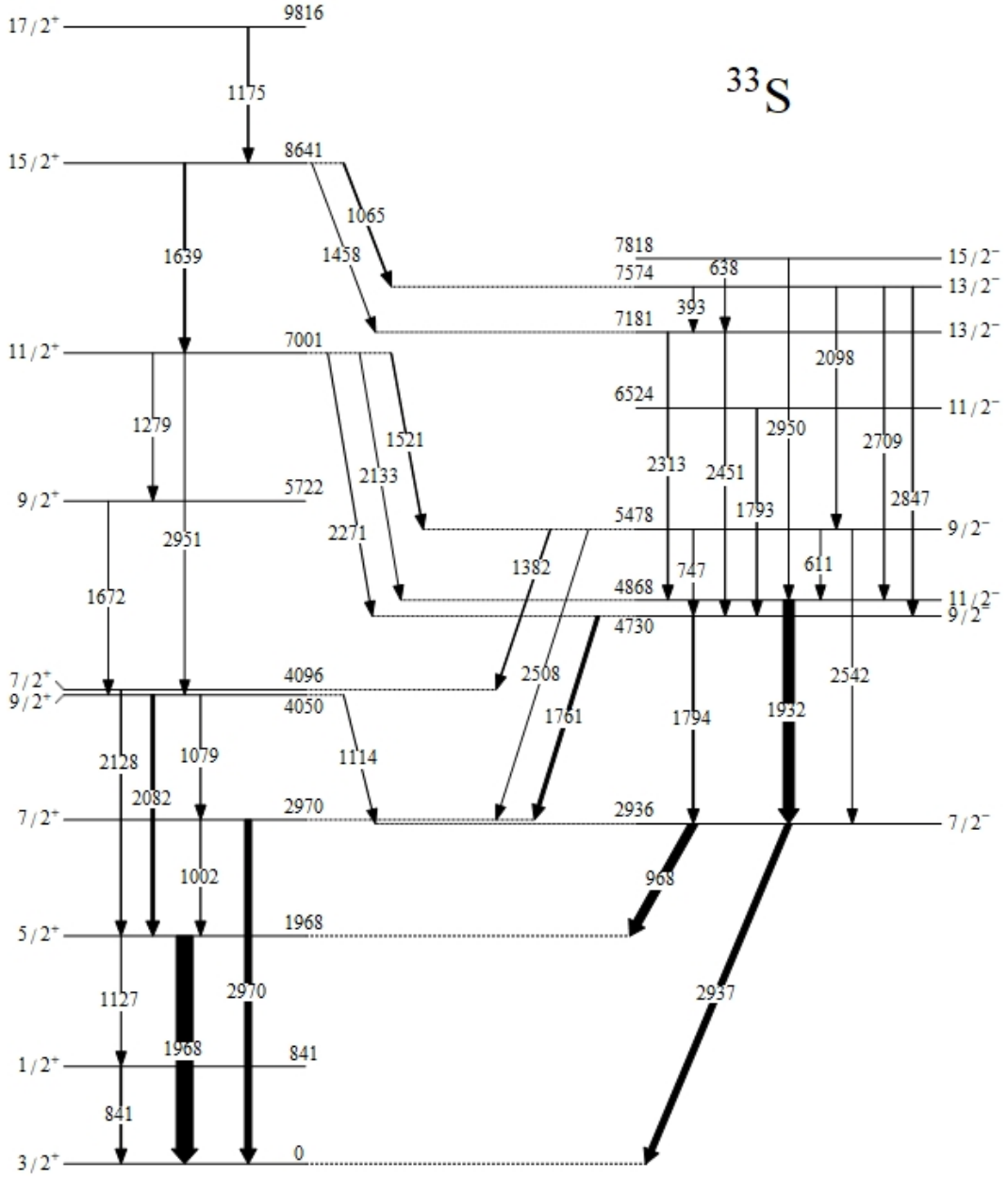

Figure 3.2: Level Scheme of ^{33}S observed in the present work. The widths of the arrows correspond to the relative intensities of γ-ray transitions.

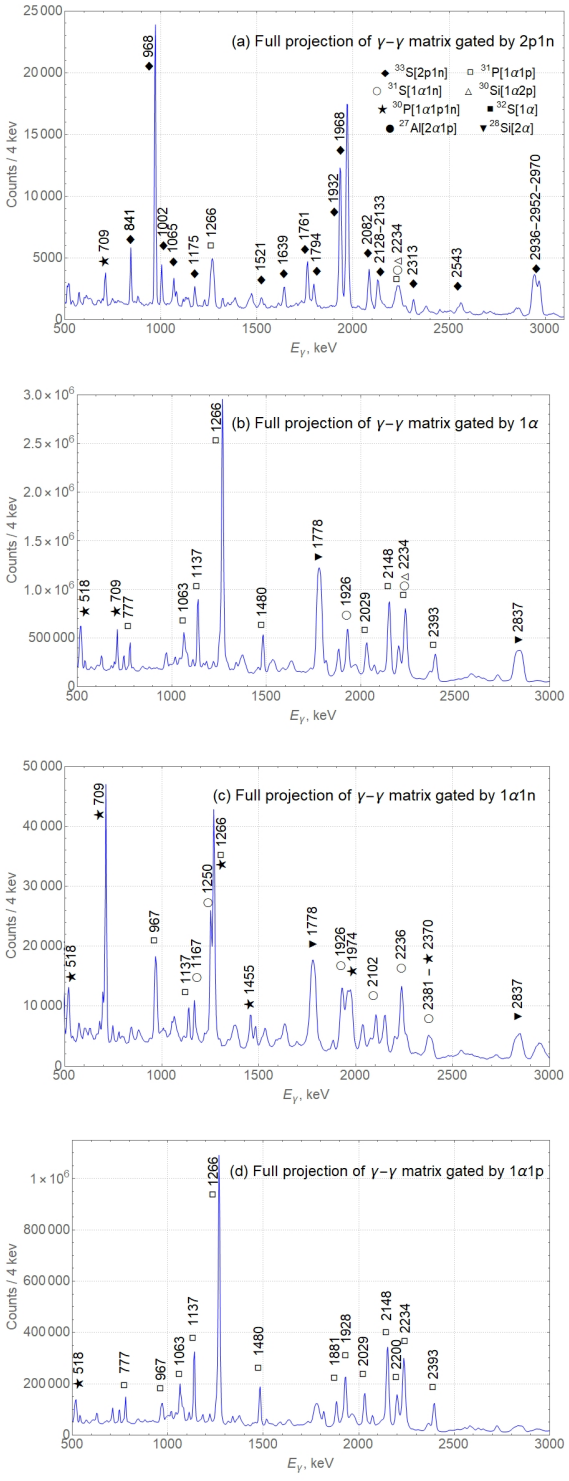

Figure 3.3: Doppler-corrected spectra obtained with GALILEO in coincidence with EUCLIDES and Newtron Wall, for the reaction ^{12}C(45MeV) + ^{24}Mg. Several conditions on the detected particles are requested.

Chapter 4

Comparison with shell model calculations.

To interpret the observed properties in ^{33}S detailed shell model calculations have been performed with the code ANTOINE [12]. For the positive parity states that involve the *sd* main shell, the USD interaction [1] is generally used. However, to be able to describe negative-parity states, an interaction that includes also the underlying *p* shell and the upper *fp* shell needs to be employed. For this purpose, the PSDPF interaction [2] has been adopted. As the *sd* matrix elements of both interactions are similar, the experimental results have been compared with the calculations using the PSDPF interaction.

In the PSDPF interaction the core considered is ^{4}He. The negative parity states result from the promotion of one nucleon from shells *p* to *sd* or *sd* to *pf*.

Figure 4.1 shows the experimental results in comparison with these calculation. There is a very good agreement between experimental and calculated positive-parity states up to the spin $11/2^+$. The calculations give the correct ordering of all levels, except the second $9/2^+$ state that is predicted above the $7/2^+$, in contrast with the experiment. On the other hand the higher spin states are predicted too high in energy. This indicates that at high spins the *sd* shell-model space is not enough for a good description of the states and that a larger valence space as excitations involving two or more particles into the *fp* shell have to be considered. This is not possible with the PSDPF interaction due to spuriousness arising from the center of mass motion.

The calculations for negative-parity states give the correct ordering of all levels, excepting the second $13/2^-$ state that is predicted above the $15/2^-$ in contrast with the experiment. Moreover the excitation energies of all levels are well reproduced. This indicates that up to spin $15/2^-$ the structure of the negative parity states involves only one excitation into *fp* orbitals.

To have a deeper insight on the calculations, the occupation numbers of protons and neutrons in the *fp* shell were extracted. The results for negative parity states are reported in the graph in Figure 4.2. For the yrast negative parity states the wave function configuration is dominated by the (unpaired) neutron excitation to the *fp* shell. On the contrast, the excitation of a proton has about 30% probability for the non yrast $9/2^-$, $11/2^-$ and reaches 50% for the second $13/2^-$. We might deduced therefore that in the latter case, the lose of pairing energy by breaking a proton pair is compensated by the strong odd proton-neutron interaction.

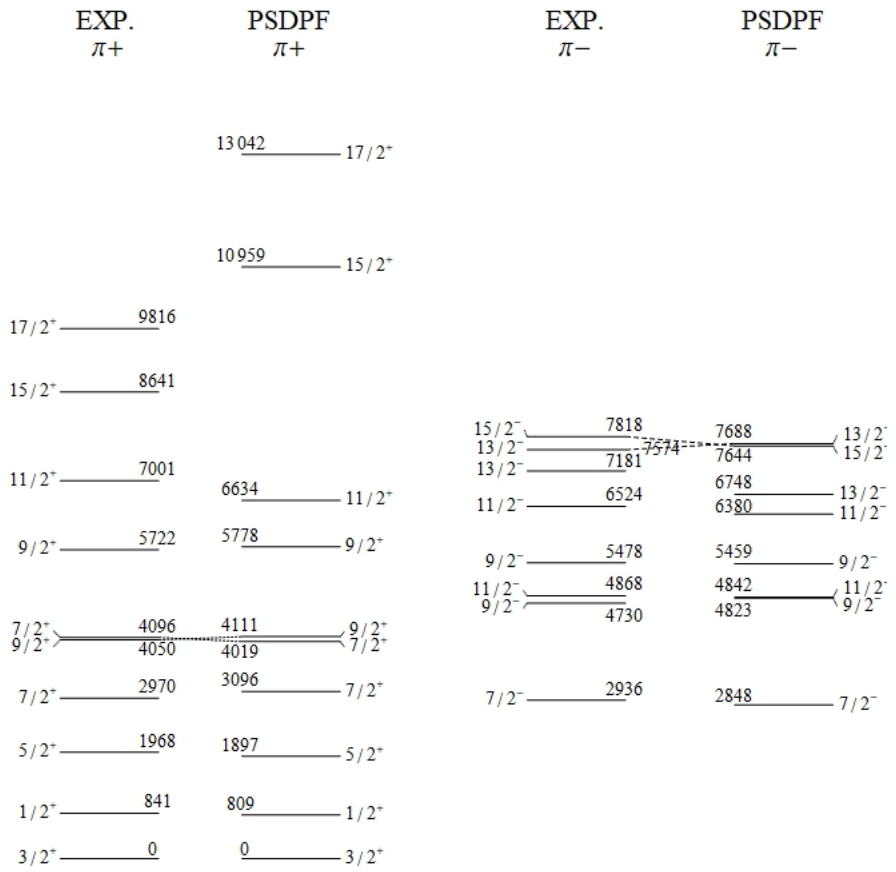

Figure 4.1: Comparison between the experimental positive and negative parity states in ^{33}S and shell-model calculated states using the PSDPF interaction.

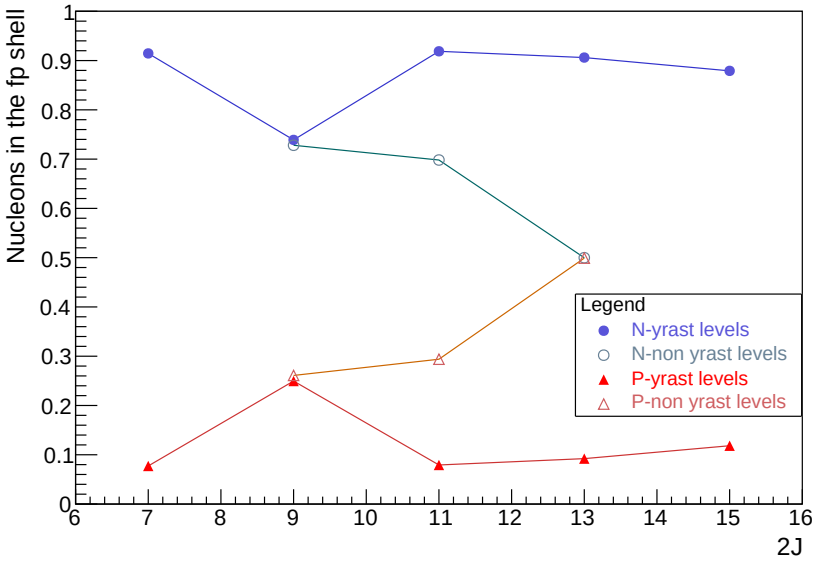

Figure 4.2: Number of protons (P) an neutrons (N) promoted to the *fp* shell for the negative parity states in ^{33}S, deduced from the shell model wave functions.

Chapter 5

Conclusions

In the present thesis the structure of ^{33}S nucleus was studied.

Excited states of ^{33}S were populated up to 10 MeV using the fusion evaporation reaction ^{24}Mg(^{12}C, 2p1n)^{33}S. The ^{12}C stable beam was delivered at 45 MeV by the XTU-Tandem Accelerator of the Legnaro National Laboratory. The detection system consisted of the γ-ray spectrometer GALILEO coupled to the Si-ball EUCLIDES and the Neutron Wall ancillary arrays. The detection of particles together with γ rays allowed the selection of the reaction channels and improvement of the correction for the Doppler effect.

Using γ-γ coincidences the level scheme of ^{33}S was reconstructed. In the present experiment the positive-parity states up to spin $17/2^+$ and the negative-parity states up to spin $15/2^-$ were observed. The relative intensity of the γ-ray transitions were determined, together with the branching ratios of the decaying levels. Where possible, the multipolarity of the γ transitions has been determined by means of the ADO ratios (Angular distribution from Orients states). The measured values are in good agreement with those from previous studies.

The level scheme was interpreted in the frame of shell-model calculations using the PSDPF interaction. The positive-parity states up to spin $11/2^+$ and all negative-parity states are very well described. At high spins the *sd* shell-model space is not large enough for a good description of the positive-parity states. A larger valence space allowing excitations of two or more particles into the *fp* shell should be considered.

Bibliography

[1] B. A. Brown *et al.*, Ann. of Phys. 182, 191 (1998).

[2] M. Bouhelal *et al.*, Nucl. Phys. A 864 113 (2011).

[3] D.Testov, J.J.Valiente-Dobon, D.Mengoni, Eur. Jour. of Phys. and Funct. Mat. 3(1), 84 (2019).

[4] D. Testov *et al.*, Eur. Phys. J.A. 2019-12714-6 (2019).

[5] I. Zanon, M. Sc. thesis, http://tesi.cab.unipd.it/61172/ (2017/2018).

[6] A. Lonardi, http://tesi.cab.unipd.it/52165/ (2014/2015).

[7] G.F. Knoll, *Radiation Detection and Measurement,* 2^{nd} *Edition*, J. Wiley & Sons, New York (1989).

[8] S. Aydin *et al.*, Phys. Rev. C 96,024315 (2017).

[9] B. Fu *et al.*, Phys. Rev. C 94, 034318 (2016).

[10] P. Mason *et al.*, Phys. Rev. C 71. 014316 (2005).

[11] M. Ionescu-Bujor *et al.*, Phys. Rev. C 73, 024310 (2006).

[12] E. Caurier and F. Nowacki, Acta Phys. Pol. B 30, 705 (1999).